Journal of Radioanalytical and Nuclear Chemistry (2025) 334:1333–1342
https://doi.org/10.1007/s10967-024-09878-9

Development and performance of a low-cost, solid-state, thermal neutron sensor with a ^{10}B converter

P. Costa[1] · J. L. Weaver[3] · M. P. Raele[1] · K. Pritchard[2] · J. B. Leão[2] · C. Domienikan[1] · N. C. Maliszewskyj[2] · F. S. da Silva[4] · W. W. Pereira[4] · F. A. Genezini[1]

Received: 30 May 2024 / Accepted: 7 November 2024 / Published online: 31 December 2024

Abstract

This study demonstrates the construction and operation of a portable, solid-state thermal neutron sensor that utilizes a photodiode coated with a thin layer of boron-10 (^{10}B). The boron layer was created using pulsed laser deposition and analyzed with neutron depth profiling (NDP) and scanning electron microscopy (SEM). The sensor's response to both thermal and cold neutrons was evaluated under varying neutron fluence rates. Additionally, the impact of the angles between the neutron beam and the sensor surface was examined. SEM results showed a porous ^{10}B film structure, while NDP indicated a nearly uniform distribution of the isotope throughout the film. The electronic signal generated by the sensor exhibited a linear response to neutron fluence rates. However, the measured intrinsic efficiencies were lower than those of commercially available gas-phase detectors, with thermal neutrons yielding an efficiency of (1.17 ± 0.01) % and cold neutrons at (1.78 ± 0.01) %. Potential design upgrades that could increase the sensor's efficiency in the future are also discussed.

Keywords PLD · Neutron sensor · Boron · Silicon photodiode · Thermal neutron · Cold neutron · PHADES · Neutron depth profile

Introduction

The helium crisis has sparked significant interest in developing more affordable alternatives to ^{3}He neutron detectors. Additionally, high-efficiency gas-filled neutron detectors used for spectroscopic or portal monitoring applications tend to be large and costly, which limits their effectiveness in nuclear threat detection and neutron dosimetry. As a result, there is a need for detectors that are relatively inexpensive, compact, portable, and reliable.

One promising alternative is a solid-state ^{10}B-based detector that uses a photodiode. The high thermal neutron absorption cross-section, short reaction product ranges, and high relative abundance of ^{10}B make this isotope an industrially appealing neutron converter [1]. Enriched boron can be applied to surfaces as ultrathin coatings, which has led to the development of neutron detectors in the form of boron-lined straws [2] and thin-layered gas detectors [3]. Other portable and compact neutron detectors with boron films have been reported in the literature [4], many of which are planar diodes coated with enriched boron (^{10}B).

A design feature often missing for the afore-cited sensors is affordability and ease of manufacturing. These gaps can be addressed by combining Pulsed Laser Deposition (PLD) for boron layer applications with an inexpensive, commercially available, large-area photodiode (e.g., Silicon photodiodes) that has characteristics suitable for nuclear applications [5]. Photodiodes have the advantage that their electronics can be compact, they can work at room temperature, and they have a very distinct response for gamma rays and charged particles, allowing for energy discrimination. Their reduced costs can offset the high cost of the needed ^{10}B materials.

✉ J. L. Weaver
jamie.weaver@nist.gov

✉ F. A. Genezini
fredzini@ipen.br

1 Nuclear and Energy Research Institute, IPEN, CNEN/SP, São Paulo, SP, Brazil

2 NIST Center for Neutron Research, National Institute of Standards and Technology, Gaithersburg, MD, USA

3 Material Measurement Laboratory, National Institute of Standards and Technology, Gaithersburg, MD, USA

4 Laboratório Nacional de Metrologia das Radiações Ionizantes LNMRI/IRD, Rio de Janeiro, RJ, Brazil

Despite recent advancements in boron-based detectors, there is still limited research on the use of photodiodes with boron converter films in a straightforward configuration. To address this gap, the present study aims to describe a thermal neutron sensor developed using an unsealed commercial silicon PIN photodiode. This photodiode consists of a p-type semiconductor, an intrinsic region, and an n-type semiconductor, and is coated with a thin layer of PLD-applied ^{10}B, as shown in Fig. 1a. The photodiode is coupled to a simple pre-amplifier.

The presented sensor's characterization was conducted using well-established thermal and cold neutron fluence rates at the Brazilian Metrology Laboratory of Ionizing Radiations and the NIST Center for Neutron Research (NCNR). Additionally, the boron layer was analyzed for thickness and homogeneity using Neutron Depth Profiling (NDP) and Scanning Electron Microscopy (SEM). All uncertainties are reported with a confidence interval of 68%.

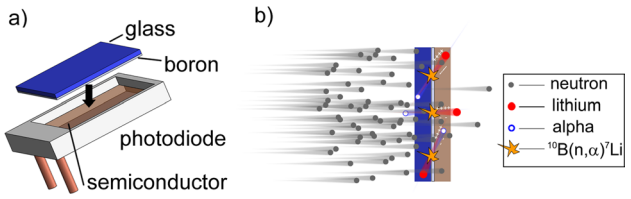

Fig. 1 Detector design: **a** illustration of the proposed detector assembly; **b** neutrons interacting with boron, resulting in the formation of energetic particles, which generate electron–hole pairs

Methods

Sensor design

The neutron-sensitive portion of the sensor relies on the reaction of neutrons with ^{10}B, Fig. 1b. The reaction is prompt, and it has two pathways: a ground state reaction and a reaction with excited state products(*) that decay to a ground state. A total of four daughter products and a gamma-ray can be formed, see Eqs. 1 and 2:

$$93.7\% : {}^{10}\mathrm{B} + \mathrm{n}_{\text{cold or thermal}} \rightarrow {}^{4}\mathrm{He}\ (1472\ \mathrm{keV}) + ({}^{7}\mathrm{Li}^{*}\ (839\ \mathrm{keV}) \rightarrow \gamma(480\ \mathrm{keV})) \quad (1)$$

$$6.3\% : {}^{10}\mathrm{B} + \mathrm{n}_{\text{cold or thermal}} \rightarrow {}^{4}\mathrm{He}\ (1776\ \mathrm{keV}) + {}^{7}\mathrm{Li}\ (1013\ \mathrm{keV}) \quad (2)$$

The produced charged particles (ions) that reach the semiconductor volume lose energy by Coulombic scattering, forming electron–hole pairs. These pairs can be collected in the semiconductor contacts by applying a bias voltage. The induced charge produces an image charge in the contact that is integrated and measured by an external preamplifier and accompanying electronics (e.g., MCA analyzer or digital counter).

The full neutron sensor prototype includes the photodiode, the ^{10}B-coated glass slide placed on the photodiode with the boron layer in contact with the photodiode, and an in-house electronic suite [5, 6]. The photodiode/slide assembly was positioned inside an aluminum box to reduce electronic noise. The applied bias voltage was 18 V.

The boron layer was produced with a femtosecond Pulsed Laser Deposition (PLD) system [7], depicted in Fig. 2, using a boron target enriched in ^{10}B at 96% (American Elements, USA). Femtosecond lasers are more effective at atomizing

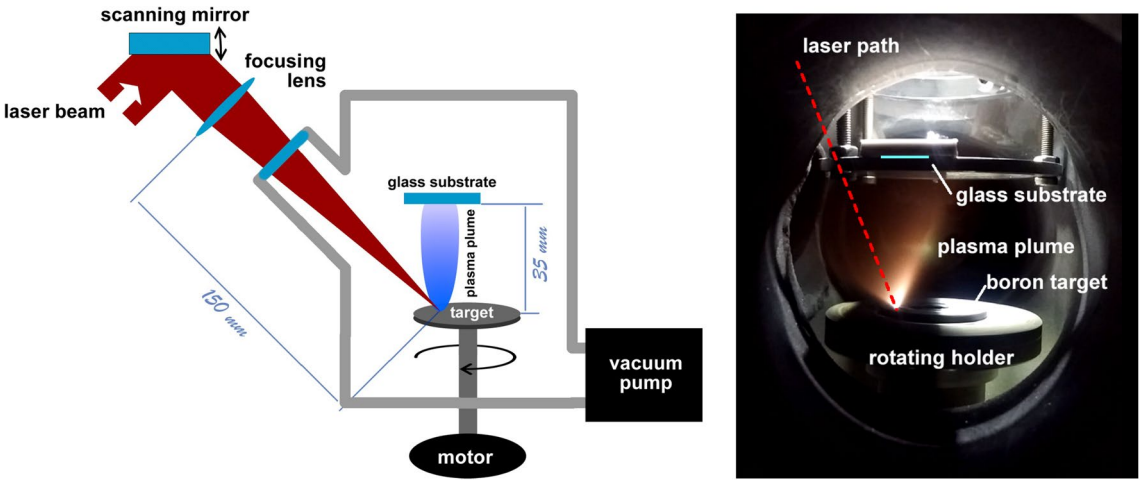

Fig. 2 Schematic illustration PLD setup and a photograph during the deposition

the ablated material, promoting smooth film growth. The laser energy applied was (177 ± 6) μJ per pulse during 75 min to achieve a thickness between 2 μm and 3 μm as proposed in [7, 22]. The deposition was performed on a glass coverslips measuring 10 mm × 10 mm × 0.15 mm; the same dimensions of the photodiode active area (Fig. 3a, b). The glass slide was then positioned over the photodiode with the side of the boron layer oriented to the photodiode's active area. This assembly has the advantage that a replacement can be made for the diode in case of device damage while keeping the ^{10}B film. The photodiode (Hamamatsu, S3590-09) was acquired from the manufacturer with the absence of the epoxy resin layer on the active area. This was necessary to avoid absorption of the alpha (α) and ^{7}Li daughter products in the epoxy resin. The aluminum case was used to shield the detector from light and is permissive to neutrons (Fig. 3c).

^{10}B film characterization

Cold neutron depth profiling

Cold neutron depth profiling (cNDP) was used to investigate the homogeneity of ^{10}B in the film's volume. NDP is a nominally nondestructive analytical technique that involves exposing a sample, kept under vacuum or in an inert gas, to a beam of thermal or cold neutrons (schematic shown in Fig. 4a, reproduced with permission from [8]) [9–11]. In an NDP experiment, selected isotopes absorb neutrons, forming unstable compound nuclei that undergoes fission, producing charged particles with specific initial energies. These particles lose energy as they move through the material(s), and, depending on their type and energy and the material characteristics, they may either be stopped within the material(s) or exit the material's surface [9]. The number and residual energy of the exited charged particles are detected and analyzed to create distribution profiles of the parent isotope within the material. For more details, see the Supporting Information (SI) and [11–13]. The isotope profile measured by NDP for this study was ^{10}B. The fission reaction products detected are those listed in Eqs. 1 and 2.

The NDP spectra in this study were acquired at the cNDP station on neutron guide 5 (NG5) at the NCNR [11]. A circular aperture made of 0.5 mm thick polytetrafluoroethylene (PTFE) with a 3.0 mm diameter opening was mounted to an Al disk with a large (> 30 mm) hole in its center (see Fig. 4a). The reported NDP results are the average distribution of ^{10}B across the non-PTFE covered material surface area and is relative to the diameter of the aperture opening. The charged ^{10}B nuclear reaction products (Eq. 1, 2 and Fig. 4) were detected using a circular transmission-type silicon surface barrier detector that was positioned ≈ 120 mm from the sample surface. [11]

^{10}B depth profiles were measured at three locations on the film: at the center, at the upper right corner, and at the lower left corner (see SI, relative to designating the uncoated sample). An additional profile of the film support without the ^{10}B film was collected as the background spectra. Each spot measured was irradiated at a near constant cold neutron fluence rate of (≈ 1.22×10^{9} neutrons cm^{-2} s^{-1}), with any variations being corrected via neutron monitor data during data reduction. The experiments were conducted under vacuum, and with a detector dead time of ≈ 0.008%. The profiles were collected for ≈ 1200 s per spot.

NDP data analysis focused on the ^{4}He* reaction product (93.7% branching ratio, 1472.42 keV) due to its relatively high-count rate and small number of interferences from other particle profiles. Details of data analysis can be found in the SI, Sect. "Introduction". Please note that the ^{10}B concentrations herein reported are estimates as the true density of the film and its quantitative porosity are not known. The profiles were corrected for instrument deadtime, sample self-shielding, and overlaps with the ^{4}He (1776.53 keV) and ^{7}Li (840.01 keV) profiles. A correction was not applied for the ^{7}Li* (1013.50 keV) profile interference due to difficulty in calculating the profiles' contribution to the ^{4}He profiles. The data shown in Fig. 2a that is beyond 2.10 μm include a mix of ^{4}He* and ^{7}Li profiles. This overlap does not significantly affect the ^{4}He profiles but may influence accurate determination of film thickness. Presented data has been binned to the resolution of the NDP detector (≈ 19 keV at the time of data collection).

SEM

High-contrast SEM images were captured using a Zeiss Ultra 60 Field Emission Scanning Electron Microscope at the NIST Center for Nanoscale Science and Technology (CNST, NIST) with an in-lens secondary detector (Fig. 4b). The sample was imaged in cross-section after being cut and mounted vertically. All images were acquired at a working distance of approximately 5.5 mm, with an accelerating voltage of 2.0 kV and a 30.0 mm aperture. The film was divided into 14 regions for thickness evaluation, yielding an average

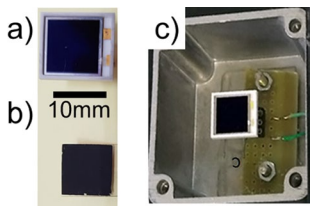

Fig. 3 Photograph of: **a** photodiode; **b** boron film over glass slipcover and **c** detector mounted inside an aluminum casing

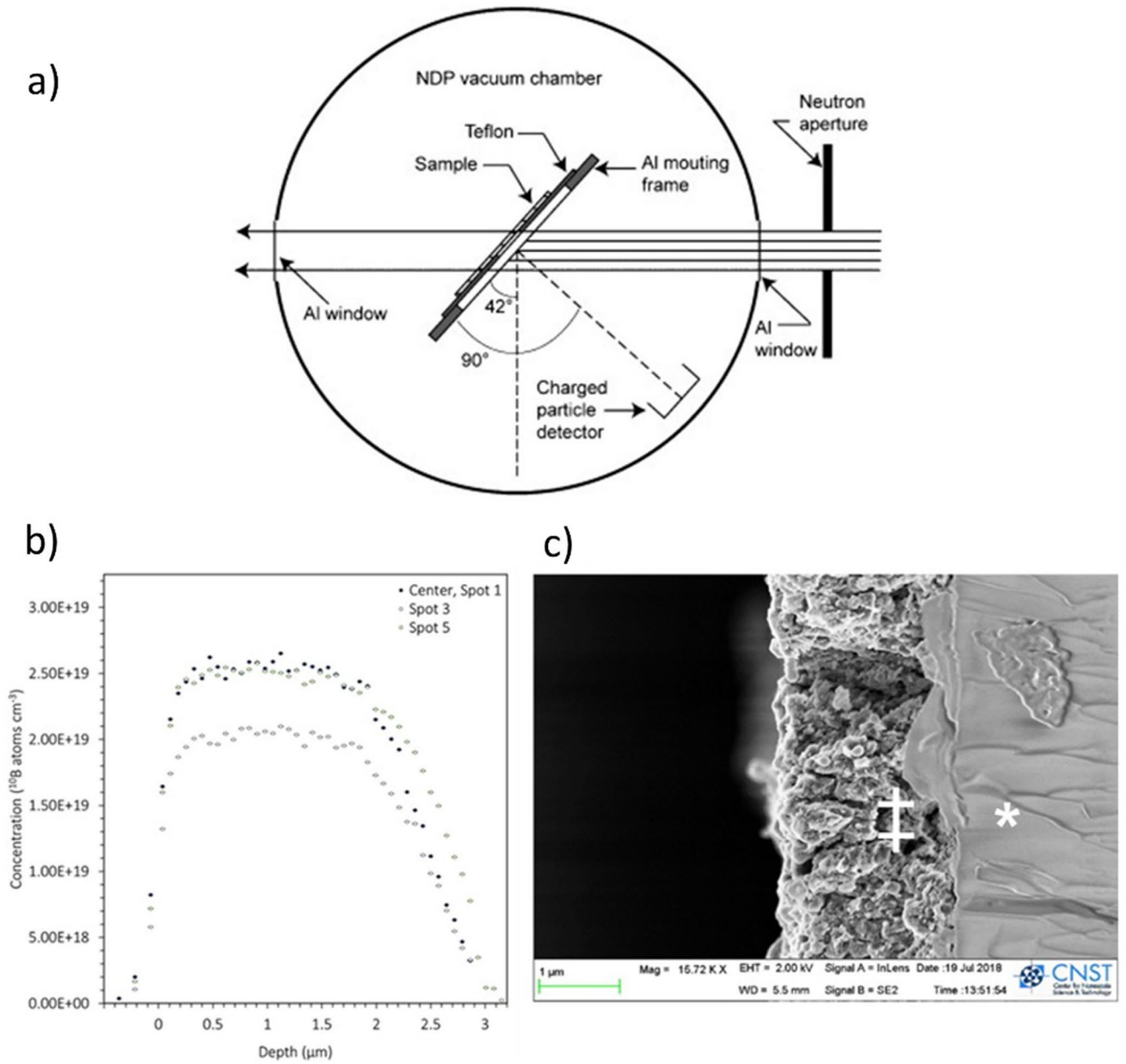

Fig. 4 **a** Schematic of NIST NDP chamber. Reproduced with permission from [8]. **b** NDP profiles from three different spots on a test film (spot 1, 3, and 5; see SI Fig. 2 for more details). Uncertainity bars in **b** may be smaller than the data points on the graph and are based on experimental counting statistics and propagated through the binning calculation. **c** SEM image of the borated film (‡) on a glass support (*)

of (2.04 ± 0.53) μm (see SI, Sect. "Methods"), consistent with values obtained from NDP profiles.

Sensor performance tests

Characterization of the thermal neutron sensor was performed using both thermal and monochromatic cold neutrons. The cross section of ^{10}B for cold neutrons with energy of $(48{,}666.2 \pm 0.6) \times 10^{-4}$ meV [15] is 8631×10^{-24} cm^2. This is $2.25\times$ higher than the cross section for thermal neutrons (3837×10^{-24} cm^2). The following studies with both thermal and cold neutron sources were conducted:

(a) *Neutron response* Verify the sensor's ability to discriminate a neutron event from other background signals and to check spectral shape. Measurements were completed with the prototype's surface perpendicular to the neutron incidence direction (here called 0° position).

(b) *Reproducibility* Repeat measurements with the same acquisition system to obtain estimate of statistical variation.
(c) *Angular response* Varying the incidence angle of the neutron beam to investigate changes in the effective neutron capture probability.

Count rate Obtain rate count measurements with different irradiation times at 0° position.Details of these experiments are presented in the following sections.

Gamma-rays response experiment

An initial experiment was conducted to verify the gamma-ray response of the prototype using a ^{60}Co source. The source was positioned on top of the closed aluminum casing (Fig. 2). The amplitude of the gamma-ray signals corresponded to a cut-off around channel 30 in the MCA, indicating that the gamma-ray contribution falls within the electronic noise region of the spectra (see SI, Sect. "Results").

Thermal neutron experiments

The neutron sensor was characterized by thermal neutrons at the Brazilian Metrology Laboratory of Ionizing Radiations (LNMRI). This facility has a standard thermal neutron fluence rate facility designed to provide uniform neutron irradiations for the calibration of small neutron sensors and individual dosimeters. The fluence rate is obtained by moderating the neutrons emitted from four, 596 GBq ^{241}Am-Be sources in a structure built with blocks consisting of paraffin mixed with high-purity carbon graphite [14, 15]. The source-to-sensor could be ranged from 25 to 200 cm (see SI, Sect. "Discussion").

All measurements were conducted at a source-to-sensor distance of 50 cm to avoid possible damage to the detection system. As the ^{241}Am-Be source has a mixed neutron fluence rate (thermal, fast, and epithermal), the fluence rate of the thermal neutron in the boron layer was simulated by Monte Carlo method (code MCNPX, [17]) with the fluence rate of thermal neutron for the distance of 50 cm. The calculated thermal contribution (< 0.5 eV) in the spectrum value was 65.3%, this corresponds to an expected thermal fluence rate of (470 ± 4) cm^{-2} s^{-1} [15].

Parameters performed in this setup were:

(a) *Neutron response* incidence at 0°, distance of 50 cm for 60 min. (Fig. 5a).
(b) *Reproducibility* incidence at 0°, fixed 50 cm distance, $n = 10$ measures, each lasting 10 min (Fig. 5b).
(c) *Angular* incidence at 0°, 30°, 60° and 90° for 15 min at each angle (Fig. 5c).
(d) *Count rate* incidence at 0°, 50 cm distance position where the neutron fluence was varied using incremented irradiation times (5 min to 60 min, Fig. 5d).

The prototype's intrinsic efficiency (ε_{int}) was calculated using a count rate obtained from the angular coefficient of six measurements, with times ranging from 5 to 60 min, at a distance of 50 cm from the radiation source. The count rate was (331 ± 2) min^{-1}, associated with the thermal neutron fluence rate of (470 ± 4) neutrons (herein n) cm^{-2} s^{-1} [15] at the same position. Using Eq. 3, [16] the calculated intrinsic efficiency of the sensor is (1.17 ± 0.01) %.

$$\varepsilon_{int} = \frac{number\ of\ neutrons\ recorded}{number\ of\ incident\ neutrons\ on\ detector} \quad (3)$$

Cold neutron experiments

The characterization of the neutron detection system was performed using the PHADES (Polarized ^{3}He and Detector Experiment Station) cold neutron beam at NCNR [17]. PHADES is a test detector/sensor facility with a monochromatic neutron beam with energy of 4.86662 (6) meV. The neutron fluence rate is approximately 2.0×10^6 n cm^{-2} s^{-1} with vertical divergence of 1°. The sensor was be placed on a standard Huber goniometer with ± 22° tilt and ± 10 mm translation. [18]

The cold neutron beam was collimated using two borated aluminum masks with 5 mm × 20 mm apertures spaced 1 m apart. In addition, a borated glass attenuator (neutron transmission (≈ 15%) was positioned in front of this collimator to reduce the neutron fluence rate so that the system dead time was negligible. The distance between the fluence rate and sensor (photodiode plus boron) was ≈ 70 cm with the photodiode positioned on the Huber base.

Parameters performed in this setup were:

(a) *Neutron response* prototype response at the 0° position.
(b) *Count rate* varying the fluence rate at the 0° position.
(c) *Angular* varying the angle to −90° to 90°, steps of 5°- and 10-min counting times.
(d) *Long-term reproducibility* collecting data for 10 min followed by a pause in counting for 10 min over a period of 10 h at the 0° position.

The sensor's intrinsic efficiency can be obtained using the neutron fluence rate, measured with a calibrated ^{3}He detector and correct due to the use of a neutron glass attenuator. The fluence rate on the sensor surface is $(1.07 \pm 0.09) \times 10^4$ cm^{-2} s^{-1}.

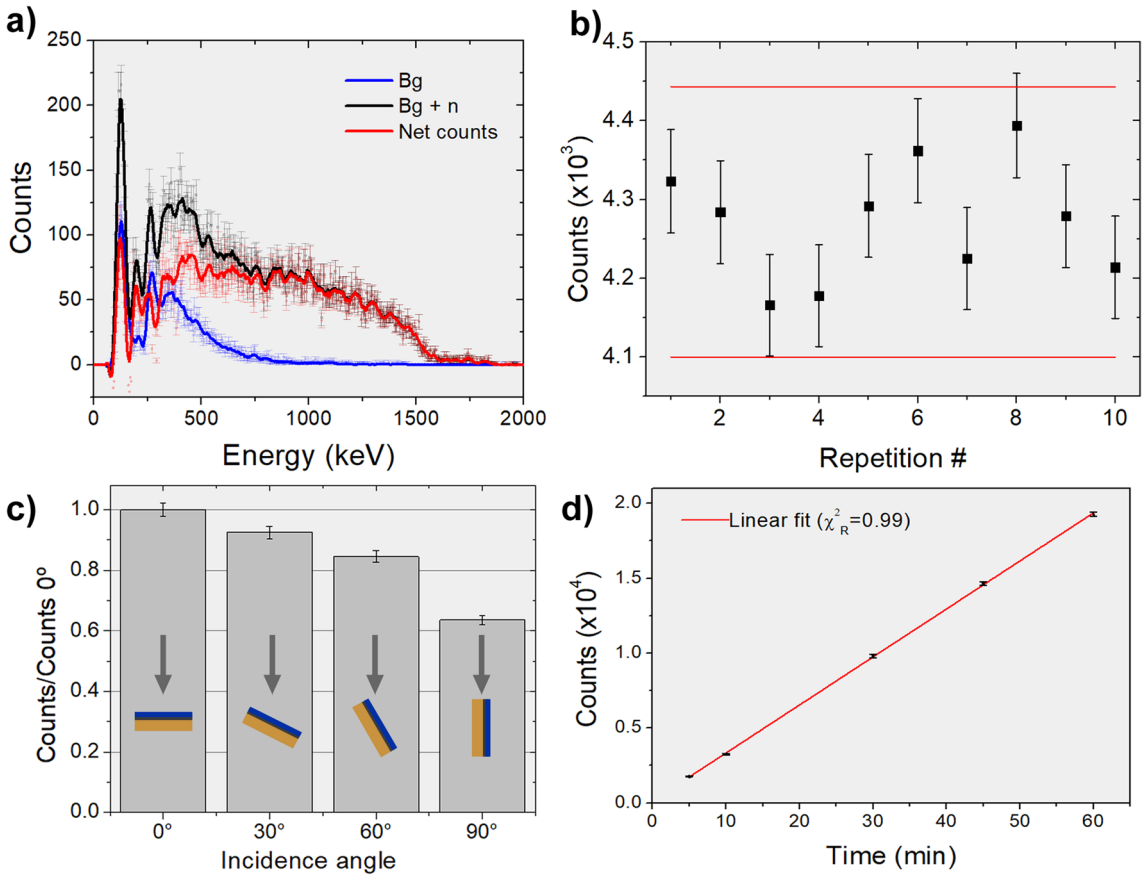

Fig. 5 **a** Experimental recorded spectra, background (B_g), thermal neutrons flux (n) and net counts; **b** Thermal neutron reproducibility measurements repeated 10 times with time acquisition of 10 min (Gross counts), red lines represents 95% confidence interval; **c** Counts versus angle position of the neutron sensor prototype with time acquisition of 15 min; **d** Counts as a function of time

Results

^{10}B film thickness, morphology, and isotopic loading consistency

The NDP profiles of the three regions suggest some variation in the overall thickness of the boron layer across the surface of the film with an approximate average thickness of ≈ 2.0 µm. This thickness is within uncertainty of the average thickness measured by SEM. The concentration of ^{10}B for all measured spots is approximately the same until a depth of 1.4 µm to 1.5 µm. At this depth, the concentration appears to decrease at a near linear rate. The decreasing concentration features are 1.0 µm to ≈ 0.75 µm in width, which is larger than the < 50 nm resolution of the NIST-NDP instrument for the ^{4}He recoil particle from the ^{10}B,*n* reaction [11, 13] and may be resulting from roughness at the support/film interface. This roughness can be seen in the micrograph shown in Fig. 4b. From this same image it is also apparent that the film is porous with, what appears to be, an open pore structure.

Neutron detection performance

Thermal neutrons Silicon detectors exhibit effective annealing at room temperature after a few days [19]. An investigation was conducted to determine if repeated measurements taken at short intervals would lead to a decrease in sensor efficiency. Figure 5a shows the experimental spectra collected from the sensor at a source-to–sensor distance of 50 cm. Repeat measurements as a function of the number of times count (*N*) is shown in (Fig. 5b) and were conducted on the same neutron flux. The black line represents the range region adopted from the repetitive measurements' dispersion. The repetitive rate (*Re*) value was calculated using Eq. 4 (from [20]) where *t* (student-t distribution) and *S* is the standard deviation. The range region is defined in Eq. 5, where X_{medium} is the average. The *t*-value is 2.26 (nine degrees of freedom; 95% of confidence) resulting in a repetitive rate value of 172 counts.

$$Re = \pm t.S \tag{4}$$

$$X_{medium} - Re < experimentaldata < X_{medium} + Re \tag{5}$$

The angular dependence of the neutron prototype is shown in Fig. 5c. The higher intensity is seen at 0° as expected and decreases as the prototype is rotated about the incident beam. The linearity response was made by varying the neutron fluency in different irradiation times, as the divergence of the fluence rate is small and does not allow variation in distance. This data is displayed in Fig. 5d.

Cold neutrons The response of the prototype to cold neutron irradiation is shown in Fig. 6a. Overall the net neutron counts (black triangles) are several orders of magnitude higher than the net background counts (green circles). Figure 6c displays the sensor's net counts as a function of angle. Figure 6d shows the linearity response of the sensor as a function of changing neutron fluency at different irradiation times. The response for gamma-rays was verified with.

Repeat measurements (N) as a function of the number of counts is shown in (Fig. 6b). These measurements were conducted on the same beamline. The black line represents the range region adopted from the repetitive rate value. The Re value was calculated using Eq. 3 (from [19]) and the range region was calculated using Eq. 4. The t-value is 2.045 (twenty-nine degrees of freedom, 95% of confidence) resulting in a repetitive rate value of 720 counts.

The intrinsic efficiency of the neutron sensor prototype was calculated using the slope of the function (linear fit) of (8810 ± 10) counts min^{-1} associated with the net number of neutrons reaching the sensor active area per minute $(6.4 \pm 0.5) \times 10^5$ n min^{-1} provided by NIST, resulting in an intrinsic efficiency of (1.37 ± 0.12) %.

The angular dependence of the neutron prototype is shown in Fig. 6c. In the alignment procedure, the photodiode detector surface was positioned parallel to the neutron beam and aligned to create an arch of rotation for the photodiode

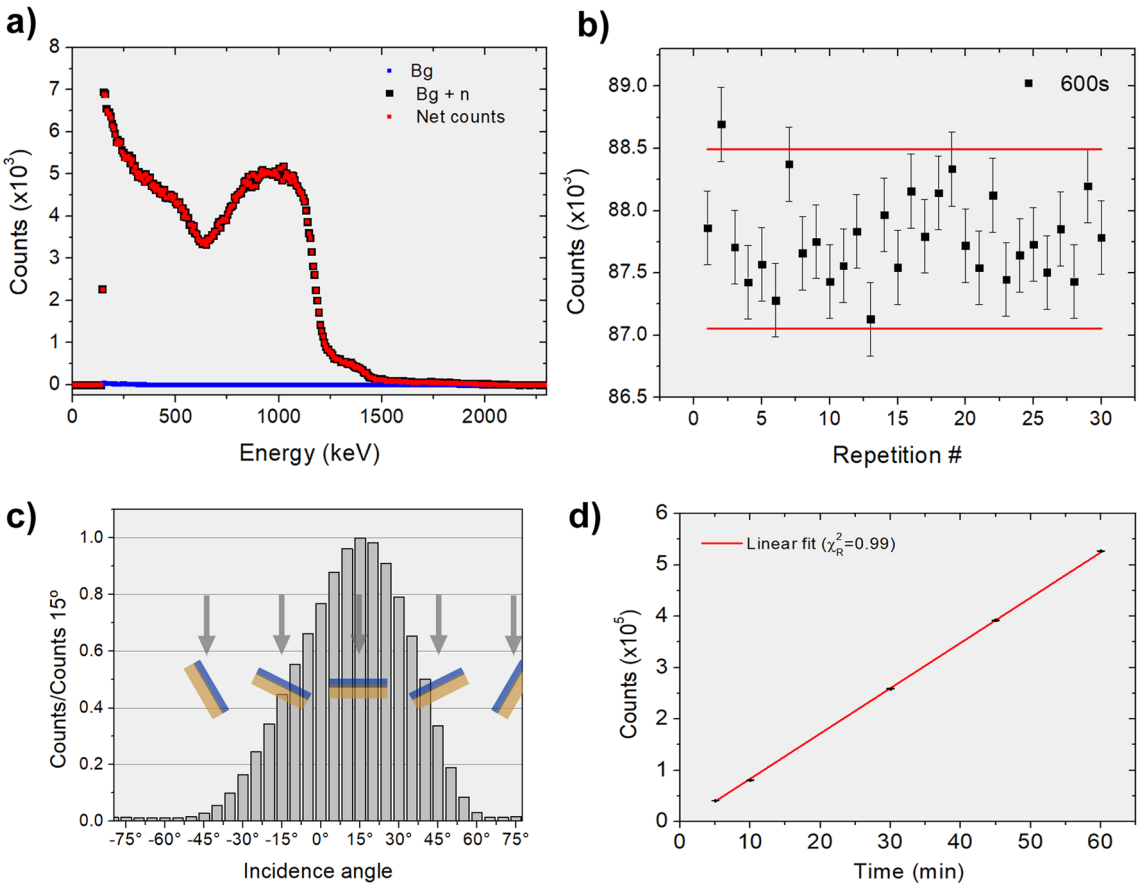

Fig. 6 **a** Experimental spectra with time acquisition of 120 s from the background (Bg), with (Bg+n) cold neutron beam and background corrected counts (Net counts). The uncertainties in the top plot are smaller than the symbols. **b** Counts as a function of the results of reproducibility measurements (Repetition number (#)), the red line represents a 95% confidence interval. **c** Counts versus angle of the neutron sensor prototype. **d** Counts as a function of time of the neutron prototype. The uncertainties are smaller than the plot symbol

about the incident beam. The asymmetry seen in the Fig. 6c could be a result of a small tilt (about 15 degrees) in the photodiode position that did not influence the overall data collection. Nevertheless, it is noted that the decrease in the value of counts between the 0° position (7.0×10^5 counts min^{-1}) in relation with the 15° (1.0×10^6 counts min^{-1}) position, is of about 30%. Previously the intrinsic efficiency was calculated to be (1.37 ± 0.12) %. A correction factor of 30% was applied in this efficiency value to adjust for this difference. The resulting intrinsic efficiency considering the correction factor is (1.78 ± 0.17) % for cold (4.87 meV) neutrons.

Discussion

NDP and SEM analyses of the ^{10}B film indicate an average thickness of (2.04 ± 0.53) µm. The film is predominantly uniform in terms of ^{10}B concentration; however, some variability in thickness is observed at the edges. Additionally, there is a near-linear decrease in ^{10}B concentration at the interface between the film and the photodiode surface, as detected by NDP. This decrease is attributed to the roughness of the ^{10}B film.

The neutron detection performance test indicates that the sensor can discriminate background counts from experimental signal counts. The photodiode response to be stable based on the experimental data collected at both cold and thermal neutron beamlines and has an intrinsic efficiency of (1.17 ± 0.01) % for thermal neutrons and (1.78 ± 0.17) % for cold neutrons. Given the goal of constructing an accessible system, commercially available low-cost electronic components were selected. Additionally, the counter was implemented using a comparator circuit based on a flip-flop design. Due to the large active area of the detector, which necessitated the use of a high-value capacitor, we estimated, through measurements using a pulser signal injected into the preamplifier, that the system's dead time is approximately 120 microseconds.. The difference between the cold neutron flux and the thermal neutron flux can lead to dead time values with up to 10% difference between the two measurements.

Another source of discrepancy arose from the ^3He detector measurement of the fluence rate. detector measurement of the fluence rate. While the exact spectral shape of the thermal neutron source is not known, it is known that the thermal component is 65.3%, the epithermal component is 21.7%, and the fast component is 11%. It is assumed that this discrepancy resulted from the ^3He detector calibration.

Comparison to other published sensors

Other, similar designs have been detailed in the literature. Comparable examples can be found in Kang et al. [21] and in the recent works of Cerasia et al. [22], Caricato et al. [23], and Provenzano et al. [24]. Kang et al. developed a sensor with a natural boron converter that was attached to a photodiode [21]. The gluing introduced an air gap of ≈ 0.3 mm that "smeared" their results. The converter material in this study was placed in direct contact with the PIN. Like the work produced by the authors of the herein paper, in [25], and in Caricato [23], Kang et al. found that converter thickness control was important to improving the sensor's efficiency. Both this study and that of Caricato et al. suggest an ≈ 2 µm thick converter layer is needed to reach good sensor efficiency.

Cerasia et al. similarly used PLD to produce enriched ^{10}B for the converter layer [22]. In Caricato et al. [23], the carbon fiber or aluminum supported converter material detailed in [22] was tested with thermal neutrons and the intrinsic efficiency was estimated to be approximately 1.7%. This work has been extended to a "sandwich" type sensor consisting of two layers and an efficiency closer to 3.5% [24]. Cold neutron tests were not completed in these studies. Cerasia et al.'s thermal neutron-based efficiency values for the single sensor design were slightly higher than the intrinsic efficiency measured for the single PIN sensor herein detailed. This could be due to several factors, as the sensors have several differences beyond how the converter material was formed (*e.g.*, deposition surface, different detection and electronic systems).

Possible improvements

One feature that may be relevant is the orientation of the substrate to the detector, which may influence the efficiency results as the sensors detailed in [22–24] have the orientation of converter material – substrate (carbon fiber or aluminum) – detector, while the herein described sensor has an orientation of substrate (glass) – converter material – detector. The presence of the glass substrate (150 µm thick [7]) facing the neutron source could cause neutron scattering, thus decreasing the number of neutrons interacting with the converter material and reducing the sensor's efficiency. Other causes of the limited performance of the sensor's efficiency may be the presence of neutron absorbing impurities in the converter layer or the presence of thicker regions of the converter which may stop some charged particles from reacting with the photodiode. Research into possible impurities in the layer need to be conducted and fine-tuning of the deposition system completed. Future work will also focus on placing more than one photodiode with the B converter in a row. Improvements on the electronic circuit using small

components and an optimized circuit board can reduce the sensor system size, thus expanding its possible applications. Future work could include utilizing the substrate materials suggested in [22–24] or decreasing the thickness of the support glass.

There are several options for improving the sensor's efficiency beyond optimizing the converter material. One option is using the sandwich configuration detailed in [24]. An alternative is a series or in parallel schema of sensors as suggested in the work of Gao et al. [26] for 4H-SiC PIN system. Other, new semiconductor designs have been developed to achieve an increase in neutron detection efficiency (for example see [27]). The proposed designs are based on producing photodiodes with a matrix that include microstructure patterns engraved on the substrate and subsequently filled with converting materials. In one of these sensors less < 1 mm thickness is needed with less than 5 V, and the intrinsic efficiency values above 40% have been reached. However, in the works consulted, most are based on ^{6}Li converters. In these studies, LiF was employed due to the difficulty of making films with pure Li, which is corrosive and chemically reactive and the filling of this material in microstructures is generally completed by centrifugation processes [28]. This is not an issue for the PVD ^{10}B sensor described here.

Cost estimate (materials only)

The low cost and the use of PLD in the presented sensor's production is advantages. For the construction of the thermal neutron detector the ^{10}B target (USD $3,781.30) was one of the more expensive investments while the PIN type Si photodiode (USD $224) had a lower cost burden. Even though ^{10}B is a high-cost material, in the manufacture of the film only a small amount of ^{10}B is needed, as the average range of the alpha particle in boron is in the order of 3.5 µm [22]) and the deposition region does not exceed 1 cm × 1 cm (the active area of the photodiode). One target can be utilized to manufacture more than six dozen (72) films, thus having a good cost–benefit ratio (approximately USD $53.00 for each film). The electronics associated with this photodiode are also low cost (USD $300) and have simple circuits and components that are easily accessible. The cost of a single detector system would be approximately USD $580.

Conclusion

In this study a compact, low-cost thermal neutron sensor is presented, characterized, and assessed for viability. This prototype is a compact neutron sensor and is a probable candidate for a portable sensor or be converted into a personal dosimeter following further development. The low cost and the use of PLD in its production are advantages that can make this sensor very attractive. For the construction of the thermal neutron sensor a commercially available PIN type Si photodiode was utilized for charged particle detection, which was coated with a ^{10}B enriched film manufactured by PLD. The film was ≈ 2.0 µm, below the average range of the alpha particle in from the ^{10}B, n reaction is in the order of 3.5 µm to 4.0 µm,. The intrinsic efficiency was determined to be (1.17 ± 0.01) % for thermal neutrons and (1.78 ± 0.17) % for cold neutrons. Improvements for the sensor have been suggested and future work may include further characterization of the converter film, research into placing more than one photodiode with the boron converter in a row, and improvements on associated electronics.

Supplementary Information The online version contains supplementary material available at https://doi.org/10.1007/s10967-024-09878-9.

Acknowledgements We would like to thank the National Council for Scientific and Technological Development (CNPq) for the projects (870240/1997-8 and Sisfóton 440228/2021-2). Certain trade names and company products are identified to adequately specify the experimental procedure. In no case does such identification imply recommendation or endorsement by the National Institute of Standards and Technology, nor does it imply that the products are necessarily the best for the purpose. A portion of this work was completed at the NIST Center for Neutron Research (NCNR) and the NIST Center for Nanoscale Science and Technology. Contribution of the National Institute of Standards and Technology; not subject to copyright in the United States.

Funding Material Measurement Laboratory,NIST Center for Neutron Research,Conselho Nacional de Desenvolvimento Científico e Tecnológico, 870240/1997-8, F. A. Genezini

Data availability Data can be made available upon reasonable request.

Declarations

Conflict of interest The authors declare no conflict of interests.

References

1. Kouzes RT, Lintereur AT, Siciliano ER (2015) Progress in alternative neutron detection to address the helium-3 shortage. Nucl Instrum Methods Phys Res Sect A 784:172–175
2. Lacy JL, Athanasiades A, Shehad N, Austin R, Martin C (2002) Novel neutron detector for high rate imaging applications. In: 2002 IEEE nuclear science symposium conference record, IEEE, Vol. 1, pp 392-396
3. Andersen K, Bigault T, Birch J, Buffet J, Correa J, Hall-Wilton R, Hultman L, Höglund C, Guérard B, Jensen J (2013) 10B multigrid proportional gas counters for large area thermal neutron detectors. Nucl Instrum Methods Phys Res Sect A 720:116–121
4. Pietropaolo A, Angelone M, Bedogni R, Colonna N, Hurd A, Khaplanov A, Murtas F, Pillon M, Piscitelli F, Schooneveld E (2020) Neutron detection techniques from µeV to GeV. Phys Rep 875:1–65
5. Costa P, Raele MP, Domienikan C, Madi Filho T, Zahn GS, Genezini FA (2019) Characterization of a portable thermal neutron

detector. In: Proceedings of the INAC 2019: international nuclear atlantic conference. Nuclear new horizons: fueling our future
6. Domienikan C, Costa P, Genezini FA, Zahn GS (2017) Low-cost amplifier for alpha detection with photodiode
7. Costa P, Raele MP, Machado NG, Silva AF, Vieira ND, Genezini FA, Samad RE (2019) Boron film laser deposition by ultrashort pulses for use as neutron converter material. Appl Phys A 125:1–8
8. Nagpure SC, Downing RG, Bhushan B, Babu S, Cao L (2011) Neutron depth profiling technique for studying aging in Li-ion batteries. Electrochim Acta 56(13):4735–4743
9. Ziegler J, Cole G, Baglin J (1972) Technique for determining concentration profiles of boron impurities in substrates. J Appl Phys 43(9):3809–3815
10. Downing R, Fleming R, Langland J, Vincent D (1983) Neutron depth profiling at the national bureau of standards. Nucl Instrum Methods Phys Res 218(1–3):47–51
11. Downing R, Lamaze G, Langland J, Hwang S (1993) Neutron depth profiling: overview and description of NIST facilities. J Res Nat Inst Stand Technol 98(1):109
12. Downing R, Maki J, Fleming R (1987) Analytical applications of neutron depth profiling. J Radioanal Nucl Chem 112(1):33–46
13. Chen-Mayer HH, Lamaze GP, Coakley K, Satija SK (2003) Two aspects of thin film analysis: boron profile and scattering length density profile. Nucl Instrum Methods Phys Res Sect A 505(1–2):531–535
14. Astuto A, Salgado A, Leite S, Patrão K, Fonseca E, Pereira W, Lopes R (2014) Thermal neutron calibration channel at LNMRI/IRD. Radiat Prot Dosim 161(1–4):185–189
15. Astuto A, Patrão KCS, Fonseca ES, Pereira WW, Lopes RT (2016) New thermal neutron calibration channel at LNMRI/IRD. In: Journal of physics: conference series, IOP publishing: Vol. 733, p 012080
16. Knoll GF (2010) Radiation detection and measurement. John Wiley & Sons, Hoboken
17. NIST (2023) Multi-purpose test station - PHADES. https://www.nist.gov/ncnr/multi-purpose-test-station-phades. Accessed 30 Oct 2024
18. Watson S, Krycka K, Erwin R, Watson K, Krycka and Erwin R. https://ncnr.nist.gov/instruments/instdev.html. Accessed 06 Oct 2023
19. Lindström G (2003) Radiation damage in silicon detectors. Nucl Instrum Methods Phys Res Sect A 512(1–2):30–43
20. Zanobini A, Sereni B, Catelani M, Ciani L (2016) Repeatability and reproducibility techniques for the analysis of measurement systems. Measurement 86:125–132
21. Kang K, Jeon H, Kim G, Park H, Hyun H, Kah D (2014) Response of a photodiode coupled with boron for neutron detection. J Korean Phys Soc 65:1374–1378
22. Cesaria M, Lorusso A, Caricato AP, Finocchiaro P, Amaducci S, Martino M, Aziz MR, Calcagnile L, Perrone A, Quarta G (2020) 10 B-based films grown by pulsed laser deposition for neutron conversion applications. Appl Phys A 126:1–11
23. Caricato AP, Cesaria M, Finocchiaro P, Amaducci S, Longhitano F, Provenzano C, Marra M, Martino M, Aziz MR, Serra A (2022) Thermal neutron conversion by high purity 10B-enriched layers: PLD-growth, thickness-dependence and neutron-detection performances. Eur Phys J Plus 137(4):431
24. Provenzano C, Marra M, Caricato AP, Finocchiaro P, Amaducci S, Longhitano F, Martino M, Poma GE, Quarta G (2023) Development of a high-efficiency device for thermal neutron detection using a sandwich of two high-purity 10B enriched layers. Sensors 23(24):9831
25. Costa P, Raele MP, Yoriyaz H, Siqueira PT, Zahn GS, Genezini FA (2015) Boron film thickness determination to develop a low cost neutron using Monte Carlo method
26. Gao R, Du X, Ma W, Sun B, Ruan J, Ouyang X, Li H, Chen L, Liu L, Ouyang X (2022) Radiation tolerance analysis of 4H-SiC PIN diode detectors for neutron irradiation. Sens Actuators A 333:113241
27. Ochs T, Bellinger S, Fronk R, Henson L, Hutchins R, McGregor D (2020) Improved manufacturing and performance of the dual-sided microstructured semiconductor neutron detector (DS-MSND). Nucl Instrum Methods Phys Res Sect A 954:161696
28. Massara A, Amaducci S, Cosentino L, Longhitano F, Marchetta C, Poma GE, Ursino M, Finocchiaro P (2022) 6LiF converters for neutron detection: production procedures and detector tests. Instruments 7(1):1